Search for continuous gravitational waves from neutron stars in globular cluster NGC 6544

B. P. Abbott,[1] R. Abbott,[1] T. D. Abbott,[2] M. R. Abernathy,[3] F. Acernese,[4,5] K. Ackley,[6] C. Adams,[7] T. Adams,[8] P. Addesso,[9] R. X. Adhikari,[1] V. B. Adya,[10] C. Affeldt,[10] M. Agathos,[11] K. Agatsuma,[11] N. Aggarwal,[12] O. D. Aguiar,[13] L. Aiello,[14,15] A. Ain,[16] B. Allen,[10,18,19] A. Allocca,[20,21] P. A. Altin,[22] S. B. Anderson,[1] W. G. Anderson,[18] K. Arai,[1] M. C. Araya,[1] C. C. Arceneaux,[23] J. S. Areeda,[24] N. Arnaud,[25] K. G. Arun,[26] S. Ascenzi,[27,15] G. Ashton,[28] M. Ast,[29] S. M. Aston,[7] P. Astone,[30] P. Aufmuth,[19] C. Aulbert,[10] S. Babak,[31] P. Bacon,[32] M. K. M. Bader,[11] P. T. Baker,[33] F. Baldaccini,[34,35] G. Ballardin,[36] S. W. Ballmer,[37] J. C. Barayoga,[1] S. E. Barclay,[38] B. C. Barish,[1] D. Barker,[39] F. Barone,[4,5] B. Barr,[38] L. Barsotti,[12] M. Barsuglia,[32] D. Barta,[40] J. Bartlett,[39] I. Bartos,[41] R. Bassiri,[42] A. Basti,[20,21] J. C. Batch,[39] C. Baune,[10] V. Bavigadda,[36] M. Bazzan,[43,44] M. Bejger,[45] A. S. Bell,[38] B. K. Berger,[1] G. Bergmann,[10] C. P. L. Berry,[46] D. Bersanetti,[47,48] A. Bertolini,[11] J. Betzwieser,[7] S. Bhagwat,[37] R. Bhandare,[49] I. A. Bilenko,[50] G. Billingsley,[1] J. Birch,[7] R. Birney,[51] S. Biscans,[12] A. Bisht,[10,19] M. Bitossi,[36] C. Biwer,[37] M. A. Bizouard,[25] J. K. Blackburn,[1] C. D. Blair,[52] D. G. Blair,[52] R. M. Blair,[39] S. Bloemen,[53] O. Bock,[10] M. Boer,[54] G. Bogaert,[54] C. Bogan,[10] A. Bohe,[31] C. Bond,[46] F. Bondu,[55] R. Bonnand,[8] B. A. Boom,[11] R. Bork,[1] V. Boschi,[20,21] S. Bose,[56,16] Y. Bouffanais,[32] A. Bozzi,[36] C. Bradaschia,[21] P. R. Brady,[18] V. B. Braginsky,[50,*] M. Branchesi,[57,58] J. E. Brau,[59] T. Briant,[60] A. Brillet,[54] M. Brinkmann,[10] V. Brisson,[25] P. Brockill,[18] J. E. Broida,[61] A. F. Brooks,[1] D. A. Brown,[37] D. D. Brown,[46] N. M. Brown,[12] S. Brunett,[1] C. C. Buchanan,[2] A. Buikema,[12] T. Bulik,[62] H. J. Bulten,[63,11] A. Buonanno,[31,64] D. Buskulic,[8] C. Buy,[32] R. L. Byer,[42] M. Cabero,[10] L. Cadonati,[65] G. Cagnoli,[66,67] C. Cahillane,[1] J. Calderón Bustillo,[65] T. Callister,[1] E. Calloni,[68,5] J. B. Camp,[69] K. C. Cannon,[70] J. Cao,[71] C. D. Capano,[10] E. Capocasa,[32] F. Carbognani,[36] S. Caride,[72] J. Casanueva Diaz,[25] C. Casentini,[27,15] S. Caudill,[18] M. Cavaglià,[23] F. Cavalier,[25] R. Cavalieri,[36] G. Cella,[21] C. B. Cepeda,[1] L. Cerboni Baiardi,[57,58] G. Cerretani,[20,21] E. Cesarini,[27,15] S. J. Chamberlin,[73] M. Chan,[38] S. Chao,[74] P. Charlton,[75] E. Chassande-Mottin,[32] B. D. Cheeseboro,[76] H. Y. Chen,[77] Y. Chen,[78] C. Cheng,[74] A. Chincarini,[48] A. Chiummo,[36] H. S. Cho,[79] M. Cho,[64] J. H. Chow,[22] N. Christensen,[61] Q. Chu,[52] S. Chua,[60] S. Chung,[52] G. Ciani,[6] F. Clara,[39] J. A. Clark,[65] F. Cleva,[54] E. Coccia,[27,14] P.-F. Cohadon,[60] A. Colla,[80,30] C. G. Collette,[81] L. Cominsky,[82] M. Constancio, Jr.,[13] A. Conte,[80,30] L. Conti,[44] D. Cook,[39] T. R. Corbitt,[2] N. Cornish,[33] A. Corsi,[72] S. Cortese,[36] C. A. Costa,[13] M. W. Coughlin,[61] S. B. Coughlin,[83] J.-P. Coulon,[54] S. T. Countryman,[41] P. Couvares,[1] E. E. Cowan,[65] D. M. Coward,[52] M. J. Cowart,[7] D. C. Coyne,[1] R. Coyne,[72] K. Craig,[38] J. D. E. Creighton,[18] T. Creighton,[88] J. Cripe,[2] S. G. Crowder,[84] A. Cumming,[38] L. Cunningham,[38] E. Cuoco,[36] T. Dal Canton,[10] S. L. Danilishin,[38] S. D'Antonio,[15] K. Danzmann,[19,10] N. S. Darman,[85] A. Dasgupta,[86] C. F. Da Silva Costa,[6] V. Dattilo,[36] I. Dave,[49] M. Davier,[25] G. S. Davies,[38] E. J. Daw,[87] R. Day,[36] S. De,[37] D. DeBra,[42] G. Debreczeni,[40] J. Degallaix,[66] M. De Laurentis,[68,5] S. Deléglise,[60] W. Del Pozzo,[46] T. Denker,[10] T. Dent,[10] V. Dergachev,[1] R. De Rosa,[68,5] R. T. DeRosa,[7] R. DeSalvo,[9] R. C. Devine,[76] S. Dhurandhar,[16] M. C. Díaz,[88] L. Di Fiore,[5] M. Di Giovanni,[89,90] T. Di Girolamo,[68,5] A. Di Lieto,[20,21] S. Di Pace,[80,30] I. Di Palma,[31,80,30] A. Di Virgilio,[21] V. Dolique,[66] F. Donovan,[12] K. L. Dooley,[23] S. Doravari,[10] R. Douglas,[38] T. P. Downes,[18] M. Drago,[10] R. W. P. Drever,[1] J. C. Driggers,[39] M. Ducrot,[8] S. E. Dwyer,[39] T. B. Edo,[87] M. C. Edwards,[61] A. Effler,[7] H.-B. Eggenstein,[10] P. Ehrens,[1] J. Eichholz,[6,1] S. S. Eikenberry,[6] W. Engels,[78] R. C. Essick,[12] T. Etzel,[1] M. Evans,[12] T. M. Evans,[7] R. Everett,[73] M. Factourovich,[41] V. Fafone,[27,15] H. Fair,[37] X. Fan,[71] Q. Fang,[52] S. Farinon,[48] B. Farr,[77] W. M. Farr,[46] M. Favata,[92] M. Fays,[91] H. Fehrmann,[10] M. M. Fejer,[42] E. Fenyvesi,[93] I. Ferrante,[20,21] E. C. Ferreira,[13] F. Ferrini,[36] F. Fidecaro,[20,21] I. Fiori,[36] D. Fiorucci,[32] R. P. Fisher,[37] R. Flaminio,[66,94] M. Fletcher,[38] J.-D. Fournier,[54] S. Frasca,[80,30] F. Frasconi,[21] Z. Frei,[93] A. Freise,[46] R. Frey,[59] V. Frey,[25] P. Fritschel,[12] V. V. Frolov,[7] P. Fulda,[6] M. Fyffe,[7] H. A. G. Gabbard,[23] J. R. Gair,[95] L. Gammaitoni,[34] S. G. Gaonkar,[16] F. Garufi,[68,5] G. Gaur,[96,86] N. Gehrels,[69] G. Gemme,[48] P. Geng,[88] E. Genin,[36] A. Gennai,[21] J. George,[49] L. Gergely,[97] V. Germain,[8] Abhirup Ghosh,[17] Archisman Ghosh,[17] S. Ghosh,[53,11] J. A. Giaime,[2,7] K. D. Giardina,[7] A. Giazotto,[21] K. Gill,[98] A. Glaefke,[38] E. Goetz,[39] R. Goetz,[6] L. Gondan,[93] G. González,[2] J. M. Gonzalez Castro,[20,21] A. Gopakumar,[99] N. A. Gordon,[38] M. L. Gorodetsky,[50] S. E. Gossan,[1] M. Gosselin,[36] R. Gouaty,[8] A. Grado,[100,5] C. Graef,[38] P. B. Graff,[64] M. Granata,[66] A. Grant,[38] S. Gras,[12] C. Gray,[39] G. Greco,[57,58] A. C. Green,[46] P. Groot,[53] H. Grote,[10] S. Grunewald,[31] G. M. Guidi,[57,58] X. Guo,[71] A. Gupta,[16] M. K. Gupta,[86] K. E. Gushwa,[1] E. K. Gustafson,[1] R. Gustafson,[101] J. J. Hacker,[24] B. R. Hall,[56] E. D. Hall,[1] G. Hammond,[38] M. Haney,[99] M. M. Hanke,[10] J. Hanks,[39] C. Hanna,[73] J. Hanson,[7] T. Hardwick,[2] J. Harms,[57,58] G. M. Harry,[3] I. W. Harry,[31] M. J. Hart,[38] M. T. Hartman,[6] C.-J. Haster,[46] K. Haughian,[38] A. Heidmann,[60] M. C. Heintze,[7] H. Heitmann,[54] P. Hello,[25] G. Hemming,[36] M. Hendry,[38] I. S. Heng,[38] J. Hennig,[38] J. Henry,[102] A. W. Heptonstall,[1] M. Heurs,[10,19] S. Hild,[38] D. Hoak,[36] D. Hofman,[66] K. Holt,[7] D. E. Holz,[77] P. Hopkins,[91] J. Hough,[38] E. A. Houston,[38] E. J. Howell,[52] Y. M. Hu,[10] S. Huang,[74] E. A. Huerta,[103] D. Huet,[25] B. Hughey,[98] S. Husa,[104] S. H. Huttner,[38] T. Huynh-Dinh,[7] N. Indik,[10] D. R. Ingram,[39] R. Inta,[72] H. N. Isa,[38] J.-M. Isac,[60] M. Isi,[1] T. Isogai,[12]

B. R. Iyer,[17] K. Izumi,[39] T. Jacqmin,[60] H. Jang,[79] K. Jani,[65] P. Jaranowski,[105] S. Jawahar,[106] L. Jian,[52] F. Jiménez-Forteza,[104] W. W. Johnson,[2] D. I. Jones,[28] R. Jones,[38] R. J. G. Jonker,[11] L. Ju,[52] Haris K.,[107] C. V. Kalaghatgi,[91] V. Kalogera,[83] S. Kandhasamy,[23] G. Kang,[79] J. B. Kanner,[1] S. J. Kapadia,[10] S. Karki,[59] K. S. Karvinen,[10] M. Kasprzack,[36,2] E. Katsavounidis,[12] W. Katzman,[7] S. Kaufer,[19] T. Kaur,[52] K. Kawabe,[39] F. Kéfélian,[54] M. S. Kehl,[108] D. Keitel,[104] D. B. Kelley,[37] W. Kells,[1] R. Kennedy,[87] J. S. Key,[88] F. Y. Khalili,[50] I. Khan,[14] S. Khan,[91] Z. Khan,[86] E. A. Khazanov,[109] N. Kijbunchoo,[39] Chi-Woong Kim,[79] Chunglee Kim,[79] J. Kim,[110] K. Kim,[111] N. Kim,[42] W. Kim,[112] Y.-M. Kim,[110] S. J. Kimbrell,[65] E. J. King,[112] P. J. King,[39] J. S. Kissel,[39] B. Klein,[83] L. Kleybolte,[29] S. Klimenko,[6] S. M. Koehlenbeck,[10] S. Koley,[11] V. Kondrashov,[1] A. Kontos,[12] M. Korobko,[29] W. Z. Korth,[1] I. Kowalska,[62] D. B. Kozak,[1] V. Kringel,[10] B. Krishnan,[10] A. Królak,[113,114] C. Krueger,[19] G. Kuehn,[10] P. Kumar,[108] R. Kumar,[86] L. Kuo,[74] A. Kutynia,[113] B. D. Lackey,[37] M. Landry,[39] J. Lange,[102] B. Lantz,[42] P. D. Lasky,[115] M. Laxen,[7] C. Lazzaro,[44] P. Leaci,[80,30] S. Leavey,[38] E. O. Lebigot,[32,71] C. H. Lee,[110] H. K. Lee,[111] H. M. Lee,[116] K. Lee,[38] A. Lenon,[37] M. Leonardi,[89,90] J. R. Leong,[10] N. Leroy,[25] N. Letendre,[8] Y. Levin,[115] J. B. Lewis,[1] T. G. F. Li,[117] A. Libson,[12] T. B. Littenberg,[118] N. A. Lockerbie,[106] A. L. Lombardi,[119] L. T. London,[91] J. E. Lord,[37] M. Lorenzini,[14,15] V. Loriette,[120] M. Lormand,[7] G. Losurdo,[58] J. D. Lough,[10,19] H. Lück,[19,10] A. P. Lundgren,[10] R. Lynch,[12] Y. Ma,[52] B. Machenschalk,[10] M. MacInnis,[12] D. M. Macleod,[2] F. Magaña-Sandoval,[37] L. Magaña Zertuche,[37] R. M. Magee,[56] E. Majorana,[30] I. Maksimovic,[120] V. Malvezzi,[27,15] N. Man,[54] V. Mandic,[84] V. Mangano,[38] G. L. Mansell,[22] M. Manske,[18] M. Mantovani,[36] F. Marchesoni,[121,35] F. Marion,[8] S. Márka,[41] Z. Márka,[41] A. S. Markosyan,[42] E. Maros,[1] F. Martelli,[57,58] L. Martellini,[54] I. W. Martin,[38] D. V. Martynov,[12] J. N. Marx,[1] K. Mason,[12] A. Masserot,[8] T. J. Massinger,[37] M. Masso-Reid,[38] S. Mastrogiovanni,[80,30] F. Matichard,[12] L. Matone,[41] N. Mavalvala,[12] N. Mazumder,[56] R. McCarthy,[39] D. E. McClelland,[22] S. McCormick,[7] S. C. McGuire,[122] G. McIntyre,[1] J. McIver,[1] D. J. McManus,[22] T. McRae,[22] S. T. McWilliams,[76] D. Meacher,[73] G. D. Meadors,[31,10] J. Meidam,[11] A. Melatos,[85] G. Mendell,[39] R. A. Mercer,[18] E. L. Merilh,[39] M. Merzougui,[54] S. Meshkov,[1] C. Messenger,[38] C. Messick,[73] R. Metzdorff,[60] P. M. Meyers,[84] F. Mezzani,[30,80] H. Miao,[46] C. Michel,[66] H. Middleton,[46] E. E. Mikhailov,[123] L. Milano,[68,5] A. L. Miller,[6,80,30] A. Miller,[83] B. B. Miller,[83] J. Miller,[12] M. Millhouse,[33] Y. Minenkov,[15] J. Ming,[31] S. Mirshekari,[124] C. Mishra,[17] S. Mitra,[16] V. P. Mitrofanov,[50] G. Mitselmakher,[6] R. Mittleman,[12] A. Moggi,[21] M. Mohan,[36] S. R. P. Mohapatra,[12] M. Montani,[57,58] B. C. Moore,[92] C. J. Moore,[125] D. Moraru,[39] G. Moreno,[39] S. R. Morriss,[88] K. Mossavi,[10] B. Mours,[8] C. M. Mow-Lowry,[46] G. Mueller,[6] A. W. Muir,[91] Arunava Mukherjee,[17] D. Mukherjee,[18] S. Mukherjee,[88] N. Mukund,[16] A. Mullavey,[7] J. Munch,[112] D. J. Murphy,[41] P. G. Murray,[38] A. Mytidis,[6] I. Nardecchia,[27,15] L. Naticchioni,[80,30] R. K. Nayak,[126] K. Nedkova,[119] G. Nelemans,[53,11] T. J. N. Nelson,[7] M. Neri,[47,48] A. Neunzert,[101] G. Newton,[38] T. T. Nguyen,[22] A. B. Nielsen,[10] S. Nissanke,[53,11] A. Nitz,[10] F. Nocera,[36] D. Nolting,[7] M. E. N. Normandin,[88] L. K. Nuttall,[37] J. Oberling,[39] E. Ochsner,[18] J. O'Dell,[127] E. Oelker,[12] G. H. Ogin,[128] J. J. Oh,[129] S. H. Oh,[129] F. Ohme,[91] M. Oliver,[104] P. Oppermann,[10] Richard J. Oram,[7] B. O'Reilly,[7] R. O'Shaughnessy,[102] D. J. Ottaway,[112] H. Overmier,[7] B. J. Owen,[72] A. Pai,[107] S. A. Pai,[49] J. R. Palamos,[59] O. Palashov,[109] C. Palomba,[30] A. Pal-Singh,[29] H. Pan,[74] C. Pankow,[83] F. Pannarale,[91] B. C. Pant,[49] F. Paoletti,[36,21] A. Paoli,[36] M. A. Papa,[31,18,10] H. R. Paris,[42] W. Parker,[7] D. Pascucci,[38] A. Pasqualetti,[36] R. Passaquieti,[20,21] D. Passuello,[21] P. Patel,[1] B. Patricelli,[20,21] Z. Patrick,[42] B. L. Pearlstone,[38] M. Pedraza,[1] R. Pedurand,[66,130] L. Pekowsky,[37] A. Pele,[7] S. Penn,[131] A. Perreca,[1] L. M. Perri,[83] M. Phelps,[38] O. J. Piccinni,[80,30] M. Pichot,[54] F. Piergiovanni,[57,58] V. Pierro,[9] G. Pillant,[36] L. Pinard,[66] I. M. Pinto,[9] M. Pitkin,[38] M. Poe,[18] R. Poggiani,[20,21] P. Popolizio,[36] A. Post,[10] J. Powell,[38] J. Prasad,[16] V. Predoi,[91] T. Prestegard,[84] L. R. Price,[1] M. Prijatelj,[10,36] M. Principe,[9] S. Privitera,[31] R. Prix,[10] G. A. Prodi,[89,90] L. Prokhorov,[50] O. Puncken,[10] M. Punturo,[35] P. Puppo,[30] M. Pürrer,[31] H. Qi,[18] J. Qin,[52] S. Qiu,[115] V. Quetschke,[88] E. A. Quintero,[1] R. Quitzow-James,[59] F. J. Raab,[39] D. S. Rabeling,[22] H. Radkins,[39] P. Raffai,[93] S. Raja,[49] C. Rajan,[49] M. Rakhmanov,[88] P. Rapagnani,[80,30] V. Raymond,[31] M. Razzano,[20,21] V. Re,[27] J. Read,[24] C. M. Reed,[39] T. Regimbau,[54] L. Rei,[48] S. Reid,[51] D. H. Reitze,[1,6] H. Rew,[123] S. D. Reyes,[37] F. Ricci,[80,30] K. Riles,[101] M. Rizzo,[102] N. A. Robertson,[1,38] R. Robie,[38] F. Robinet,[25] A. Rocchi,[15] L. Rolland,[8] J. G. Rollins,[1] V. J. Roma,[59] R. Romano,[4,5] G. Romanov,[123] J. H. Romie,[7] D. Rosińska,[132,45] S. Rowan,[38] A. Rüdiger,[10] P. Ruggi,[36] K. Ryan,[39] S. Sachdev,[1] T. Sadecki,[39] L. Sadeghian,[18] M. Sakellariadou,[133] L. Salconi,[36] M. Saleem,[107] F. Salemi,[10] A. Samajdar,[126] L. Sammut,[115] E. J. Sanchez,[1] V. Sandberg,[39] B. Sandeen,[83] J. R. Sanders,[37] B. Sassolas,[66] P. R. Saulson,[37] O. E. S. Sauter,[101] R. L. Savage,[39] A. Sawadsky,[19] P. Schale,[59] R. Schilling,[10,*] J. Schmidt,[10] P. Schmidt,[1,78] R. Schnabel,[29] R. M. S. Schofield,[59] A. Schönbeck,[29] E. Schreiber,[10] D. Schuette,[10,19] B. F. Schutz,[91,31] J. Scott,[38] S. M. Scott,[22] D. Sellers,[7] A. S. Sengupta,[96] D. Sentenac,[36] V. Sequino,[27,15] A. Sergeev,[109] Y. Setyawati,[53,11] D. A. Shaddock,[22] T. Shaffer,[39] M. S. Shahriar,[83] M. Shaltev,[10] B. Shapiro,[42] P. Shawhan,[64] A. Sheperd,[18] D. H. Shoemaker,[12] D. M. Shoemaker,[65] K. Siellez,[65] X. Siemens,[18] M. Sieniawska,[45] D. Sigg,[39] A. D. Silva,[13] A. Singer,[1] L. P. Singer,[69] A. Singh,[31,10,19] R. Singh,[2] A. Singhal,[14] A. M. Sintes,[104] B. J. J. Slagmolen,[22] J. R. Smith,[24] N. D. Smith,[1] R. J. E. Smith,[1] E. J. Son,[129] B. Sorazu,[38] F. Sorrentino,[48] T. Souradeep,[16] A. K. Srivastava,[86] A. Staley,[41] M. Steinke,[10] J. Steinlechner,[38]

S. Steinlechner,[38] D. Steinmeyer,[10,19] B. C. Stephens,[18] R. Stone,[88] K. A. Strain,[38] N. Straniero,[66] G. Stratta,[57,58] N. A. Strauss,[61] S. Strigin,[50] R. Sturani,[124] A. L. Stuver,[7] T. Z. Summerscales,[134] L. Sun,[85] S. Sunil,[86] P. J. Sutton,[91] B. L. Swinkels,[36] M. J. Szczepańczyk,[98] M. Tacca,[32] D. Talukder,[59] D. B. Tanner,[6] M. Tápai,[97] S. P. Tarabrin,[10] A. Taracchini,[31] R. Taylor,[1] T. Theeg,[10] M. P. Thirugnanasambandam,[1] E. G. Thomas,[46] M. Thomas,[7] P. Thomas,[39] K. A. Thorne,[7] E. Thrane,[115] S. Tiwari,[14,90] V. Tiwari,[91] K. V. Tokmakov,[106] K. Toland,[38] C. Tomlinson,[87] M. Tonelli,[20,21] Z. Tornasi,[38] C. V. Torres,[88,*] C. I. Torrie,[1] D. Töyrä,[46] F. Travasso,[34,35] G. Traylor,[7] D. Trifirò,[23] M. C. Tringali,[89,90] L. Trozzo,[135,21] M. Tse,[12] M. Turconi,[54] D. Tuyenbayev,[88] D. Ugolini,[136] C. S. Unnikrishnan,[99] A. L. Urban,[18] S. A. Usman,[37] H. Vahlbruch,[19] G. Vajente,[1] G. Valdes,[88] N. van Bakel,[11] M. van Beuzekom,[11] J. F. J. van den Brand,[63,11] C. Van Den Broeck,[11] D. C. Vander-Hyde,[37] L. van der Schaaf,[11] J. V. van Heijningen,[11] A. A. van Veggel,[38] M. Vardaro,[43,44] S. Vass,[1] M. Vasúth,[40] R. Vaulin,[12] A. Vecchio,[46] G. Vedovato,[44] J. Veitch,[46] P. J. Veitch,[112] K. Venkateswara,[137] D. Verkindt,[8] F. Vetrano,[57,58] A. Viceré,[57,58] S. Vinciguerra,[46] D. J. Vine,[51] J.-Y. Vinet,[54] S. Vitale,[12] T. Vo,[37] H. Vocca,[34,35] C. Vorvick,[39] D. V. Voss,[6] W. D. Vousden,[46] S. P. Vyatchanin,[50] A. R. Wade,[22] L. E. Wade,[138] M. Wade,[138] M. Walker,[2] L. Wallace,[1] S. Walsh,[31,10] G. Wang,[14,58] H. Wang,[46] M. Wang,[46] X. Wang,[71] Y. Wang,[52] R. L. Ward,[22] J. Warner,[39] M. Was,[8] B. Weaver,[39] L.-W. Wei,[54] M. Weinert,[10] A. J. Weinstein,[1] R. Weiss,[12] L. Wen,[52] P. Weßels,[10] T. Westphal,[10] K. Wette,[10] J. T. Whelan,[102] B. F. Whiting,[6] R. D. Williams,[1] A. R. Williamson,[91] J. L. Willis,[139] B. Willke,[19,10] M. H. Wimmer,[10,19] W. Winkler,[10] C. C. Wipf,[1] H. Wittel,[10,19] G. Woan,[38] J. Woehler,[10] J. Worden,[39] J. L. Wright,[38] D. S. Wu,[10] G. Wu,[7] J. Yablon,[83] W. Yam,[12] H. Yamamoto,[1] C. C. Yancey,[64] H. Yu,[12] M. Yvert,[8] A. Zadrożny,[113] L. Zangrando,[44] M. Zanolin,[98] J.-P. Zendri,[44] M. Zevin,[83] L. Zhang,[1] M. Zhang,[123] Y. Zhang,[102] C. Zhao,[52] M. Zhou,[83] Z. Zhou,[83] X. J. Zhu,[52] M. E. Zucker,[1,12] S. E. Zuraw,[119] J. Zweizig,[1]

(LIGO Scientific Collaboration and Virgo Collaboration) and S. Sigurdsson[73]

[1]*LIGO, California Institute of Technology, Pasadena, California 91125, USA*
[2]*Louisiana State University, Baton Rouge, Louisiana 70803, USA*
[3]*American University, Washington, D.C. 20016, USA*
[4]*Università di Salerno, Fisciano, I-84084 Salerno, Italy*
[5]*INFN, Sezione di Napoli, Complesso Universitario di Monte S.Angelo, I-80126 Napoli, Italy*
[6]*University of Florida, Gainesville, Florida 32611, USA*
[7]*LIGO Livingston Observatory, Livingston, Louisiana 70754, USA*
[8]*Laboratoire d'Annecy-le-Vieux de Physique des Particules (LAPP), Université Savoie Mont Blanc, CNRS/IN2P3, F-74941 Annecy-le-Vieux, France*
[9]*University of Sannio at Benevento, I-82100 Benevento, Italy and INFN, Sezione di Napoli, I-80100 Napoli, Italy*
[10]*Albert-Einstein-Institut, Max-Planck-Institut für Gravitationsphysik, D-30167 Hannover, Germany*
[11]*Nikhef, Science Park, 1098 XG Amsterdam, Netherlands*
[12]*LIGO, Massachusetts Institute of Technology, Cambridge, Massachusetts 02139, USA*
[13]*Instituto Nacional de Pesquisas Espaciais, 12227-010 São José dos Campos, São Paulo, Brazil*
[14]*INFN, Gran Sasso Science Institute, I-67100 L'Aquila, Italy*
[15]*INFN, Sezione di Roma Tor Vergata, I-00133 Roma, Italy*
[16]*Inter-University Centre for Astronomy and Astrophysics, Pune 411007, India*
[17]*International Centre for Theoretical Sciences, Tata Institute of Fundamental Research, Bangalore 560012, India*
[18]*University of Wisconsin-Milwaukee, Milwaukee, Wisconsin 53201, USA*
[19]*Leibniz Universität Hannover, D-30167 Hannover, Germany*
[20]*Università di Pisa, I-56127 Pisa, Italy*
[21]*INFN, Sezione di Pisa, I-56127 Pisa, Italy*
[22]*Australian National University, Canberra, Australian Capital Territory 0200, Australia*
[23]*The University of Mississippi, University, Mississippi 38677, USA*
[24]*California State University Fullerton, Fullerton, California 92831, USA*
[25]*LAL, University of Paris-Sud, CNRS/IN2P3, Université Paris-Saclay, F-91898 Orsay, France*
[26]*Chennai Mathematical Institute, Chennai 603103, India*
[27]*Università di Roma Tor Vergata, I-00133 Roma, Italy*
[28]*University of Southampton, Southampton SO17 1BJ, United Kingdom*
[29]*Universität Hamburg, D-22761 Hamburg, Germany*
[30]*INFN, Sezione di Roma, I-00185 Roma, Italy*
[31]*Albert-Einstein-Institut, Max-Planck-Institut für Gravitationsphysik, D-14476 Potsdam-Golm, Germany*
[32]*APC, AstroParticule et Cosmologie, Université Paris Diderot, CNRS/IN2P3, CEA/Irfu, Observatoire de Paris, Sorbonne Paris Cité, F-75205 Paris Cedex 13, France*

[33]*Montana State University, Bozeman, Montana 59717, USA*
[34]*Università di Perugia, I-06123 Perugia, Italy*
[35]*INFN, Sezione di Perugia, I-06123 Perugia, Italy*
[36]*European Gravitational Observatory (EGO), I-56021 Cascina, Pisa, Italy*
[37]*Syracuse University, Syracuse, New York 13244, USA*
[38]*SUPA, University of Glasgow, Glasgow G12 8QQ, United Kingdom*
[39]*LIGO Hanford Observatory, Richland, Washington 99352, USA*
[40]*Wigner RCP, RMKI, H-1121 Budapest, Konkoly Thege Miklós út 29-33, Hungary*
[41]*Columbia University, New York, New York 10027, USA*
[42]*Stanford University, Stanford, California 94305, USA*
[43]*Università di Padova, Dipartimento di Fisica e Astronomia, I-35131 Padova, Italy*
[44]*INFN, Sezione di Padova, I-35131 Padova, Italy*
[45]*CAMK-PAN, 00-716 Warsaw, Poland*
[46]*University of Birmingham, Birmingham B15 2TT, United Kingdom*
[47]*Università degli Studi di Genova, I-16146 Genova, Italy*
[48]*INFN, Sezione di Genova, I-16146 Genova, Italy*
[49]*RRCAT, Indore MP 452013, India*
[50]*Faculty of Physics, Lomonosov Moscow State University, Moscow 119991, Russia*
[51]*SUPA, University of the West of Scotland, Paisley PA1 2BE, United Kingdom*
[52]*University of Western Australia, Crawley, Western Australia 6009, Australia*
[53]*Department of Astrophysics/IMAPP, Radboud University Nijmegen,*
P.O. Box 9010, 6500 GL Nijmegen, Netherlands
[54]*Artemis, Université Côte d'Azur, CNRS, Observatoire Côte d'Azur, CS 34229, Nice cedex 4, France*
[55]*Institut de Physique de Rennes, CNRS, Université de Rennes 1, F-35042 Rennes, France*
[56]*Washington State University, Pullman, Washington 99164, USA*
[57]*Università degli Studi di Urbino "Carlo Bo", I-61029 Urbino, Italy*
[58]*INFN, Sezione di Firenze, I-50019 Sesto Fiorentino, Firenze, Italy*
[59]*University of Oregon, Eugene, Oregon 97403, USA*
[60]*Laboratoire Kastler Brossel, UPMC-Sorbonne Universités, CNRS, ENS-PSL Research University,*
Collège de France, F-75005 Paris, France
[61]*Carleton College, Northfield, Minnesota 55057, USA*
[62]*Astronomical Observatory Warsaw University, 00-478 Warsaw, Poland*
[63]*VU University Amsterdam, 1081 HV Amsterdam, Netherlands*
[64]*University of Maryland, College Park, Maryland 20742, USA*
[65]*Center for Relativistic Astrophysics and School of Physics, Georgia Institute of Technology,*
Atlanta, Georgia 30332, USA
[66]*Laboratoire des Matériaux Avancés (LMA), CNRS/IN2P3, F-69622 Villeurbanne, France*
[67]*Université Claude Bernard Lyon 1, F-69622 Villeurbanne, France*
[68]*Università di Napoli "Federico II", Complesso Universitario di Monte S.Angelo, I-80126 Napoli, Italy*
[69]*NASA/Goddard Space Flight Center, Greenbelt, Maryland 20771, USA*
[70]*RESCEU, University of Tokyo, Tokyo, 113-0033, Japan*
[71]*Tsinghua University, Beijing 100084, China*
[72]*Texas Tech University, Lubbock, Texas 79409, USA*
[73]*The Pennsylvania State University, University Park, Pennsylvania 16802, USA*
[74]*National Tsing Hua University, Hsinchu City, 30013 Taiwan, Republic of China*
[75]*Charles Sturt University, Wagga Wagga, New South Wales 2678, Australia*
[76]*West Virginia University, Morgantown, West Virginia 26506, USA*
[77]*University of Chicago, Chicago, Illinois 60637, USA*
[78]*Caltech CaRT, Pasadena, California 91125, USA*
[79]*Korea Institute of Science and Technology Information, Daejeon 305-806, Korea*
[80]*Università di Roma "La Sapienza", I-00185 Roma, Italy*
[81]*University of Brussels, Brussels 1050, Belgium*
[82]*Sonoma State University, Rohnert Park, California 94928, USA*
[83]*Center for Interdisciplinary Exploration & Research in Astrophysics (CIERA), Northwestern University,*
Evanston, Illinois 60208, USA
[84]*University of Minnesota, Minneapolis, Minnesota 55455, USA*
[85]*The University of Melbourne, Parkville, Victoria 3010, Australia*
[86]*Institute for Plasma Research, Bhat, Gandhinagar 382428, India*
[87]*The University of Sheffield, Sheffield S10 2TN, United Kingdom*
[88]*The University of Texas Rio Grande Valley, Brownsville, Texas 78520, USA*

[89] Università di Trento, Dipartimento di Fisica, I-38123 Povo, Trento, Italy

[90] INFN, Trento Institute for Fundamental Physics and Applications, I-38123 Povo, Trento, Italy

[91] Cardiff University, Cardiff CF24 3AA, United Kingdom

[92] Montclair State University, Montclair, New Jersey 07043, USA

[93] MTA Eötvös University, "Lendulet" Astrophysics Research Group, Budapest 1117, Hungary

[94] National Astronomical Observatory of Japan, 2-21-1 Osawa, Mitaka, Tokyo 181-8588, Japan

[95] School of Mathematics, University of Edinburgh, Edinburgh EH9 3FD, United Kingdom

[96] Indian Institute of Technology, Gandhinagar Ahmedabad Gujarat 382424, India

[97] University of Szeged, Dóm tér 9, Szeged 6720, Hungary

[98] Embry-Riddle Aeronautical University, Prescott, Arizona 86301, USA

[99] Tata Institute of Fundamental Research, Mumbai 400005, India

[100] INAF, Osservatorio Astronomico di Capodimonte, I-80131 Napoli, Italy

[101] University of Michigan, Ann Arbor, Michigan 48109, USA

[102] Rochester Institute of Technology, Rochester, New York 14623, USA

[103] NCSA, University of Illinois at Urbana-Champaign, Urbana, Illinois 61801, USA

[104] Universitat de les Illes Balears, IAC3—IEEC, E-07122 Palma de Mallorca, Spain

[105] University of Białystok, 15-424 Białystok, Poland

[106] SUPA, University of Strathclyde, Glasgow G1 1XQ, United Kingdom

[107] IISER-TVM, CET Campus, Trivandrum, Kerala 695016, India

[108] Canadian Institute for Theoretical Astrophysics, University of Toronto, Toronto, Ontario M5S 3H8, Canada

[109] Institute of Applied Physics, Nizhny Novgorod 603950, Russia

[110] Pusan National University, Busan 609-735, Korea

[111] Hanyang University, Seoul 133-791, Korea

[112] University of Adelaide, Adelaide, South Australia 5005, Australia

[113] NCBJ, 05-400 Świerk-Otwock, Poland

[114] IM-PAN, 00-956 Warsaw, Poland

[115] Monash University, Victoria 3800, Australia

[116] Seoul National University, Seoul 151-742, Korea

[117] The Chinese University of Hong Kong, Shatin, NT, Hong Kong SAR, China

[118] University of Alabama in Huntsville, Huntsville, Alabama 35899, USA

[119] University of Massachusetts-Amherst, Amherst, Massachusetts 01003, USA

[120] ESPCI, CNRS, F-75005 Paris, France

[121] Università di Camerino, Dipartimento di Fisica, I-62032 Camerino, Italy

[122] Southern University and A&M College, Baton Rouge, Louisiana 70813, USA

[123] College of William and Mary, Williamsburg, Virginia 23187, USA

[124] Instituto de Física Teórica, University Estadual Paulista/ICTP South American Institute for Fundamental Research, São Paulo, São Paulo 01140-070, Brazil

[125] University of Cambridge, Cambridge CB2 1TN, United Kingdom

[126] IISER-Kolkata, Mohanpur, West Bengal 741252, India

[127] Rutherford Appleton Laboratory, HSIC, Chilton, Didcot, Oxon OX11 0QX, United Kingdom

[128] Whitman College, 345 Boyer Avenue, Walla Walla, Washington 99362 USA

[129] National Institute for Mathematical Sciences, Daejeon 305-390, Korea

[130] Université de Lyon, F-69361 Lyon, France

[131] Hobart and William Smith Colleges, Geneva, New York 14456, USA

[132] Janusz Gil Institute of Astronomy, University of Zielona Góra, 65-265 Zielona Góra, Poland

[133] King's College London, University of London, London WC2R 2LS, United Kingdom

[134] Andrews University, Berrien Springs, Michigan 49104, USA

[135] Università di Siena, I-53100 Siena, Italy

[136] Trinity University, San Antonio, Texas 78212, USA

[137] University of Washington, Seattle, Washington 98195, USA

[138] Kenyon College, Gambier, Ohio 43022, USA

[139] Abilene Christian University, Abilene, Texas 79699, USA

We describe a directed search for continuous gravitational waves in data from the sixth initial LIGO science run. The target was the nearby globular cluster NGC 6544 at a distance of ≈2.7 kpc. The search

---

[*] Deceased.

covered a broad band of frequencies along with first and second frequency derivatives for a fixed sky position. The search coherently integrated data from the two LIGO interferometers over a time span of 9.2 days using the matched-filtering $\mathcal{F}$-statistic. We found no gravitational-wave signals and set 95% confidence upper limits as stringent as 6.0×10^{-25} on intrinsic strain and 8.5×10^{-6} on fiducial ellipticity. These values beat the indirect limits from energy conservation for stars with characteristic spin-down ages older than 300 years and are within the range of theoretical predictions for possible neutron-star ellipticities. An important feature of this search was use of a barycentric resampling algorithm which substantially reduced computational cost; this method is used extensively in searches of Advanced LIGO and Virgo detector data.

I. INTRODUCTION

The LIGO Scientific Collaboration and Virgo Collaboration have undertaken numerous searches for continuous gravitational waves (GW). None has yet detected a signal, but many have placed interesting upper limits (ULs) on possible sources. These searches have generally been drawn from one of three types.

Targeted searches are aimed at a single known pulsar, with a known precise timing solution. The first search for continuous waves, using data from the first initial LIGO science run (S1), was of this type [1], and subsequent searches have probed the Crab and Vela pulsars, among others [2–7]. A number of these most recent searches have been able to set direct upper limits on GW emission comparable to or stricter than the indirect "spin-down limits" (derived from energy conservation, as well as the distance from Earth of the target, its gravitational-wave frequency, and the frequency's first derivative, the spin down) for a few of the pulsars searched.

All-sky searches, as their name suggests, survey the entire sky for neutron stars not seen as pulsars. These are very computationally costly, searching over wide frequency bands and covering large ranges of spin-down parameters [8–17]. The latest of these have incorporated new techniques to cover possible binary parameters as well [18]. Recent all-sky searches have set direct upper limits close to indirect upper limits derived from galactic neutron-star population simulations [19].

Directed searches sit between these two extremes. As in the all-sky case, their targets are neutron stars not seen as pulsars, so that the frequency and other parameters are unknown. They focus, however, on a known sky location (and therefore a known detector-frame Doppler modulation). This directionality allows for searching over a wide range of frequencies and frequency derivatives while remaining much cheaper computationally than an all-sky search without sacrificing sensitivity. This approach was first used in a search for the accreting neutron star in the low-mass x-ray binary Sco X-1 [9,20,21].

The search for the central compact object in the supernova remnant Cassiopeia A (Cas A) [22] was the first directed search for a young neutron star without electromagnetically detected pulsation, motivated by the idea that young neutron stars might be promising emitters of continuous GW. The Cas A search [22] set upper limits on GW strain which beat an indirect limit derived from energy conservation and the age of the remnant [23] over a wide frequency band. Other directed searches have since followed in its footsteps, using different data analysis methods, for supernova 1987A and unseen neutron stars near the galactic Center [21,24]. Most methodologically similar to this search and the S5 Cas A search was a recent search for nine supernova remnants [25], which also used fully coherent integration over observation times on the order of 10 days.

In this article, we describe a search of data from the sixth initial LIGO science run (S6) for potential young isolated neutron stars with no observed electromagnetic pulsations in the nearby ($d \approx 2.7$ kpc) globular cluster NGC 6544. Globular clusters are unlikely to contain young neutron stars, but in these dense environments older neutron stars may be subject to debris accretion (see Sec. II C) or other events which could render them detectable as gravitational-wave sources. This particular globular cluster was chosen so that a computationally feasible coherent search similar to [22] could beat the age-based indirect limits on GW emission.

The search did not find a GW signal, and hence the main result is a set of upper limits on strain amplitude, fiducial ellipticity, and r-mode amplitude α, similar to those presented in [22]. An important new feature of the search described here was use of a barycentric resampling algorithm which substantially reduced computational cost, allowing a search over a larger parameter space using a longer coherence time (see Sec. II D). This barycentric resampling method is used extensively in searches of Advanced LIGO and Virgo detector data.

This article is structured as follows: In Sec. II we present the method, implementation, and results of the search. The upper limits set in the absence of a signal are presented in Sec. III, and the results are discussed in Sec. IV.

II. SEARCHES

A. Data selection

The sixth initial LIGO science run (S6) extended from July 7, 2009 21:00:00 UTC (GPS 931035615) to October 21, 2010 00:00:00 UTC (GPS 971654415) and included two initial LIGO detectors with 4-km arm lengths, H1 at LIGO Hanford Observatory near Hanford, Washington and L1 at LIGO Livingston Observatory near Livingston, Louisiana.

After optimization at fixed computing cost determined an optimum coherence time of 9.2 days (see Sec. II D), two different methods were used to determine which data would be searched, producing two different 9.2-day stretches. Both were searched, allowing for the comparison of search results between them.

The first method was to look for the most sensitive average data from S6. This was done by taking nine week-long data samples from each detector spaced roughly 55 days apart, giving nine evenly spaced weeks throughout the duration of S6. The data samples used are shown in Table I. We chose four representative frequencies (100, 200, 400, and 600 Hz) and generated joint-detector strain noise power spectral densities (PSDs) in 1-Hz bands about these frequencies, using 0.01-Hz binning. The sensitivity h_{sens} was then taken to be

$$h_{\text{sens}}^{j} = \left(\frac{1}{\sqrt{(1/100) \cdot \sum_{i=0}^{100} (S_h^i(f_i))^{-1}}} \right)_j \qquad (1)$$

where $S_h^i(f)$ represents the PSD value of the ith bin, at frequency f_i, and the index j runs from 1 through 4 and represents the four representative frequencies (note that this is not an actual estimate of detectable strain). At all four frequencies, detector sensitivity improved as the run progressed. Using this figure of merit, it was found that the final nine days of S6 yielded the most sensitive data stretch

TABLE I. The weeks sampled to find the most sensitive S6 data. Times are given both in GPS and UTC calendar dates.

Label	GPS start	GPS end	Dates (UTC)
	S6 sampling times		
Week 1	931053000	931657800	Jul 8–15, 2009
Week 2	936053000	936657800	Sep 3–10, 2009
Week 3	941053000	941657800	Oct 31–Nov 7, 2009
Week 4	946053000	946657800	Dec 28, 2009–Jan 4, 2010
Week 5	951053000	951657800	Feb 24–Mar 3, 2010
Week 6	956053000	956657800	Apr 23–30, 2010
Week 7	961053000	961657800	Jun 20–27, 2010
Week 8	966053000	966657800	Aug 17–24, 2010
Week 9	971053000	971657800	Oct 14–21, 2010

for all four frequencies: October 11–20, 2010 (GPS 970840605–971621841).

An alternate data selection scheme [22,25], which takes detector duty cycle into account, is to maximize the figure of merit

$$\sum_{k,f} \frac{1}{S_h(f)} \qquad (2)$$

where $S_h(f)$ represents the strain noise power spectral density at frequency f in the kth short Fourier transform (SFT), and the sum is taken across all frequencies f in the search band and all SFTs in a given 9.2-day (see Sec. II D below) observation time. The SFT format is science-mode detector data split into 1800s segments, band-pass filtered from 40–2035 Hz, Tukey windowed in the time domain, and Fourier transformed. This method favored a different data stretch: July 24–August 2, 2010 (GPS 964007133–964803598). This second data stretch had slightly worse average sensitivity than the first, but a higher detector livetime: our first (October) data set contained 374 SFTs (202 from Hanford and 172 from Livingston) with average sensitivity $h_{\text{sens}}^{200 \text{ Hz}} = 1.92 \times 10^{-23}$; the second (July–August) data set contained 642 SFTs (368 from Hanford and 274 from Livingston) with average sensitivity $h_{\text{sens}}^{200 \text{ Hz}} = 1.95 \times 10^{-23}$.

B. Analysis method

The analysis was based on matched filtering, the optimal method for detecting signals of known functional form. To obtain that form we assumed that the potential target neutron star did not glitch (suffer an abrupt frequency jump) or have significant timing noise (additional, possibly stochastic, time dependence of the frequency) [26] during the observation. We also neglected third and higher derivatives of the GW frequency, based on the time span and range of $\dot{f}$ and $\ddot{f}$ (the first two derivatives) covered. The precise expression for the interferometer strain response $h(t)$ to an incoming continuous GW also includes amplitude and phase modulation by the changing of the beam patterns as the interferometer rotates with the Earth. It depends on the source's sky location and orientation angles, as well as on the parameters of the interferometer. The full expression can be found in [27].

The detection statistic used was the multi-interferometer $\mathcal{F}$-statistic [28], based on the single-interferometer $\mathcal{F}$-statistic [27]. This combines the results of matched filters for the signal in a way that is computationally fast and nearly optimal [29]. Assuming Gaussian noise, $2\mathcal{F}$ is drawn from a χ^2 distribution with 4 degrees of freedom.

We used the implementation of the $\mathcal{F}$-statistic in the LALSuite package [30]. In particular most of the computing power of the search was spent in the

ComputeFStatistic_v2 program. Unlike the version used in preceding methodologically similar searches [22,25], this one implements an option to use a barycentric resampling algorithm which significantly speeds up the analysis.

The method of efficiently computing the $\mathcal{F}$-statistic by barycentering and fast-Fourier transforming the data was first proposed in [27]. Various implementations of this method have been developed and used in previous searches, such as [31–33]. Here we are using a new LALSuite [30] implementation of this method, which evolved out of [33], and which will be described in more detail in a future publication. It converts the input data into a heterodyned, down-sampled time series weighted by antenna-pattern coefficients, and then resamples this time series at the Solar System barycenter using an interpolation technique. The resampled time series is then Fourier transformed to return to the frequency domain, and from there the $\mathcal{F}$-statistic is calculated. For this search, both single-detector and multidetector $\mathcal{F}$-statistics were calculated (see the vetoes section below).

Timing tests run on a modern processor (ca. 2011) showed that the resampling code was more than 24 times faster in terms of seconds per template per SFT. This improvement, by more than an order of magnitude, was used to perform a deeper search over a wider parameter space than previously possible for the computational cost incurred (see target selection and search parameters below).

C. Target selection

Unlike previous directed searches, this one targets a globular cluster. Since stars in globular clusters are very old, it is unlikely that a young neutron star will be found in such an environment. However, some neutron stars are known to be accompanied by debris disks [34] and even planets [35–37]. In the densely populated core of a globular cluster, close encounters may stimulate bombardment episodes as debris orbits are destabilized, akin to cometary bombardments in our Solar System when the Oort cloud is perturbed [38]. A neutron star which has recently accreted debris could have it funneled by the magnetic field into mountains which relax on time scales of 10^5–10^8 years [39] and emit gravitational waves for that duration. Other mechanisms are likely to last a few years at most [40]. Hence an old neutron star could be a good gravitational-wave source with a low spin-down age.

The first step in picking a globular cluster is a figure of merit based on that for directed searches for supernova remnants [23], an indirect upper limit on gravitational-wave strain based on energy conservation and the age of the object. Here the inverse of the object age is replaced by the interaction rate of the globular cluster, which scales like density$^{(3/2)}$ times core radius^2 [38,41], reflecting the mean time since the last bombardment. It is hard to know when the most recent bombardment episode was, and thus the

constant factor out in front, but globular clusters can be ranked with respect to each other by a maximum-strain-type figure of merit

$$h_0 \propto \rho_c^{3/4} r_c/d, \tag{3}$$

where ρ_c is the globular cluster core density, r_c is the core radius, d is the distance to the cluster, and thus r_c/d is the angular radius of the core. We ranked the Harris catalog of globular clusters [42,43] by this figure of merit and looked at the top few choices, which were mainly nearby core-collapsed clusters. The closest is NGC 6397 at ≈ 2.2 kpc, but it is at high declination. This lessens the Doppler modulation of any gravitational-wave signal, making it harder to distinguish from stationary spectral line artifacts, which tend to contaminate searches at high declination near the ecliptic pole. Hence we chose the next closest, NGC 6544, which is at a declination of less than 30 degrees and only slightly further away at ≈ 2.7 kpc.

We restrict the search described below to sources for which the bombardment history corresponds to a characteristic spin-down age older than 300 years. The figure of 300 years is mainly a practical consideration: the cost of a search rises steeply for lower spin-down ages, and 300 years proved tractable for the Cas A search [22].

D. Search parameter space

An iterative method was used to generate the parameter space to be searched. Starting with an (assumed) spin-down age no younger than 300 years, a braking index $n = 5$ (see below), and the known distance to the globular cluster, we calculated the age-based indirect upper limit. This is an optimistic limit on the gravitational-wave strain h_0 which assumes that all energy lost as the target neutron star spins down is radiated away as gravitational waves [23],

$$h_0 \leq \frac{1}{d} \sqrt{\frac{5GI}{2c^3 \tau (n-1)}}. \tag{4}$$

Here d is the distance to the target, τ the assumed age of the target object, and I a fiducial moment of inertia for a neutron star (10^{38} kg $\cdot$ m^2). G and c are the gravitational constant and the speed of light, respectively. This age-based limit was then superimposed on a curve of expected upper limits in the absence of signal for the LIGO detectors, obtained from the noise PSD harmonically averaged over all of S6 and both interferometers. A running median with a 16-Hz window was further applied to smooth the curve. The curve is given by

$$h_0^{95\%} = \Theta \sqrt{\frac{S_h}{T_{\text{data}}}} \tag{5}$$

where S_h is the harmonically averaged noise, T_{data} is the coherence time (the total data livetime searched coherently), initially estimated at two weeks, and Θ is a sensitivity factor that includes a trials factor, or number of templates searched, and uncertainty in the source orientation [23]. For a directed search like ours, Θ is approximately 35 [23,44]. The intersection of this coherence-time adjusted upper limit curve and our indirect limit [Eq. (4)] gives an initial frequency band over which the indirect limit can be beaten. The braking index is related to the frequency parameters by the definition,

$$ n = \frac{f\ddot{f}}{\dot{f}^2}. \tag{6} $$

Assuming a braking index n between 2 and 7 covers most accepted neutron-star models ($n = 5$, the neutron star radiating all energy as gravitational waves via the mass quadrupole, is used to obtain the indirect limit). We allow the braking indices in these expressions to range from 2 to 7 independently, to reflect the fact that in general multiple processes are operating and $\dot{f}$ is not a simple power law. This constraint on the braking indices then produces limits on the frequency derivatives given by [23]

$$ \frac{f}{\tau} \le -\dot{f} \le \frac{f}{6\tau} \tag{7} $$

for the spin down at each frequency and

$$ \frac{2\dot{f}^2}{f} \le \ddot{f} \le \frac{7\dot{f}^2}{f} \tag{8} $$

for the second spin down at each $(f, \dot{f})$. The step sizes for frequency and its derivatives are given by the equations [33,45,46]

$$ df = \frac{2\sqrt{3m}}{\pi}\frac{1}{T_{\text{data}}}, \tag{9} $$

$$ d\dot{f} = \frac{12\sqrt{5m}}{\pi}\frac{1}{T_{\text{data}}^2}, \tag{10} $$

and

$$ d\ddot{f} = \frac{20\sqrt{7m}}{\pi}\frac{1}{T_{\text{data}}^3}, \tag{11} $$

where m is the mismatch parameter, the maximum loss of $2\mathcal{F}$ due to discretization of the frequency and derivatives [47,48]. This search used a mismatch parameter $m = 0.2$ at all stages.

From these relations the total number of templates (points in frequency parameter space) to be searched can be calculated, and with knowledge of the per-template time taken by the code (obtained from timing tests), the total computing time can be obtained. Limiting the target computing time, in our case to 1000 core months, then allows us to solve for the coherence time T_{data}, which we then feed back into Eq. (5) to begin the process anew until it iteratively converges on a parameter space and accompanying coherence time. The iterative algorithm thus balances the computational gains from resampling between the use of a longer coherence time (giving better sensitivity) and the expansion of the parameter space over which the indirect limit can be beaten (caused by the improved sensitivity). The result for the globular cluster NGC 6544 is a search over the frequency range 92.5 to 675 Hz, with a coherence time of 9.2 days.

The peculiar velocities of globular clusters are negligible, as they represent an essentially constant Doppler shift of order 1×10^{-3}; so is velocity dispersion, which is an order of magnitude smaller. Since we search down to 300-year time scales, the acceleration of the cluster is also not an issue [49].

E. Implementation

All searches were run on the LIGO-Caltech Computing Cluster at the California Institute of Technology in Pasadena, California, under the control of the Condor queuing system for parallel processing. The search process was split into 5825 individual Condor jobs, each of which searched over a 0.1-Hz sub-band and corresponding swathes of $(\dot{f}, \ddot{f})$. The number of templates searched by each job thus varied as a function of frequency.

Each search job produced three distinct outputs. First, a record was made of all candidates with $2\mathcal{F}$ above 45.0, a choice of recording different from the fifth initial LIGO science run (S5) search which recorded the loudest 0.01% of events. This was needed because of the contamination of the S6 noise by detector artifacts, as well as limits on the disk space available and the input/output capability of the cluster file system. Second, a histogram of $2\mathcal{F}$ values for all templates searched was produced to verify that the data matched the expected chi-square distribution (described in Sec. II B above). Last, each job produced a record of the loudest (highest-$2\mathcal{F}$-valued) candidate in its 0.1-Hz band, regardless of threshold. This data were used in the setting and validation of upper limits (see Sec. III below).

F. Vetoes

A high value of $2\mathcal{F}$ is not enough to claim a detection, since instrumental artifacts lead to non-Gaussian and/or nonstationary noise in many narrow frequency bands. A variety of veto techniques was used to trim down the initial list of candidates and arrive at a final list of outliers.

TABLE II.   Search sub-bands that, due to the identified disturbances, produced an excessive number of candidates and were aborted. The 580.0 Hz sub-band had to be stopped only for the July–August run; the other six bands were vetoed in both searches.

Band	job minimum and maximum frequency (Hz)		Note
370.1	370.1	370.2	L1 output mode cleaner (OMC) jitter line
393.1	393.1	393.2	H1 calibration line
396.7	396.7	396.8	L1 calibration line
400.2	400.2	400.3	H1 OMC quad photodiode (QPD) line
403.8	403.8	403.9	L1 OMC QPD line
417.1	417.1	417.2	H1 OMC QPD line
580.0	580.0	580.1	L1 2 Hz Harmonic

Six 0.1 Hz sub-bands [see Table (II)] had to be manually aborted in both searches, with a seventh aborted in the July–August search, as even with the threshold in place, they produced an excessive number of candidates. Each of these sub-bands was compared to records of known noise artifacts and disturbances in the detector, and in each case a known instrumental line was confirmed. These sub-bands were later rerun with the record of candidates disabled in order to produce histograms and loudest-outlier files for upper limit validation.

To protect against spurious noise lines, a second veto based on the $\mathcal{F}$-statistic consistency veto introduced in [15] was used. This uses the fact that an astrophysical signal should have a higher joint value of $2\mathcal{F}$ (combining data from the two interferometers) than in either interferometer alone. Recorded candidates that violate this inequality were vetoed. This is a simpler version of the more recent line veto [50].

Finally, to enforce coincidence between detectors, a single-detector threshold was employed. Since a true astrophysical signal should be present in both detectors at a significant level, any candidates passing the initial joint-detector detection criteria (see Sec. II G) also had to pass an additional threshold on the individual-detector values of $2\mathcal{F}$.

The 0.1 Hz band between 200 and 200.1 Hz was arbitrarily chosen as a test band. The joint-detector $2\mathcal{F}$ values were taken from the loudest-candidate files and used to semianalytically compute [51] an estimate of the 95% upper limit for that sub-band using the SFTs employed by the search. Sets of 1,000 software injections were performed with strengths of 100%, 80%, 60%, 40% and 20% of this estimated upper limit. The results were used to set a threshold of $2\mathcal{F} \geq 20$ in each individual detector, leading to an additional false dismissal rate of 1.5% of injections at the 95% confidence upper limit estimate (ULE). Candidates failing to meet this criterion were vetoed.

G. Detection criteria and results

The results of a mock data challenge (MDC) were used to set a detection criterion for the joint-detector $2\mathcal{F}$ value. The mock data challenge consisted of a set of 1577 artificial continuous wave (CW) signals injected into a set of real detector data from S6, which were then searched for using the same resampled $\mathcal{F}$-statistic used in the search. A survey of the loudest joint-detector $2\mathcal{F}$ value reported for background sub-bands known to be free of injected signals for the band between 200 and 240 Hz (used in a pilot MDC run) gave a mean loudest joint detector $2\mathcal{F} \approx 55$. While we cannot be sure there were zero true signals in these sub-bands, the fact that no true CW signal has ever been reported in the S6 data implies that the odds that real signals were present, in high enough number and strength to significantly alter that mean, are very low. This threshold was confirmed to be appropriate for other bands as well, via visual examination of distributions of the detection statistic in a large sampling of 0.1 Hz bins throughout the full search band and via examination of the loudest detection statistic from each 0.1 Hz sub-band for all 0.1 Hz sub-bands. Given this background level, the detection criterion was chosen to be joint detector $2\mathcal{F} \geq 60$ to maintain high efficiency and low false-alarm rate (the false-alarm rate was 3.17% in these pilot sub-bands).

With these detection criteria, a search was carried out in S6 data. The lists of all templates with joint detector $2\mathcal{F}$ greater than 45.0 were filtered for the individual detector threshold and the consistency veto, both singly and in tandem. If the loudest template failed either check, the list was used to move to the next-loudest template until the loudest template passing all thresholds and vetoes was identified. This created three sets of results (threshold only, veto only, and threshold + veto) which could all be queried independently.

The joint $2\mathcal{F}$ values for the loudest single template (passing all thresholds and vetoes) in each 0.1 Hz sub-band were collated into lists spanning 10 Hz (100 joint $2\mathcal{F}$ values per list). These lists were then parsed, and any joint $2\mathcal{F}$ values greater than the joint $2\mathcal{F}$ threshold of 60 were identified. Each such entry's corresponding template was then added to a list of outliers. This method produced a list of 168 outliers for the entirety of the search band in the October data, and a list of 155 outliers for the entirety of the search band in the July–August data.

These outliers were then tested using time shifts and extended looks. In a time shift, the frequency parameters of the outliers from each data stretch (October and July–August) were evolved forwards or backwards in time, as appropriate, and sought in the opposite data stretch, under the assumption that a true astrophysical signal should be present in both data sets for the implicitly long lived CW signals searched for here. A set of 1000 software injections (simulated signals with randomly generated parameters) underwent the same treatment to provide a baseline $2\mathcal{F}$

TABLE III. The seven candidates that passed the first round of outlier follow up. The columns give, respectively, the outlier's identifying number; the frequency of the outlier in the search; the frequency of the outlier in the follow-up data set in which it appeared; the $2\mathcal{F}$ value of the outlier in the search; the $2\mathcal{F}$ value of the outlier in the follow-up data set in which it appeared; the explanation, if any, provided by comparison with run-averaged strain histograms in conjunction with detector characterization records. For outliers due to random noise and for many instrumental artifacts, we expect the follow-up $2\mathcal{F}$ to be smaller than the originally obtained $2\mathcal{F}$, in contrast to true signals for which $2\mathcal{F}$ should increase with observation time.

Outlier	Search f (Hz)	Follow-up f (Hz)	Search $2\mathcal{F}_J$	Follow-up $2\mathcal{F}_J$	Artifact, if any
			July–August data		
27	192.4907	192.4956	612.969	300.712	Hardware injection
74	392.2232	392.2315	189.903	173.787	Clock noise
77	394.0231	394.0307	228.268	197.300	Digital line
			October data		
27	192.4195	192.4313	875.575	484.254	Hardware injection
79	403.6424	403.8612	114.626	61.331	——
85	417.0394	417.1384	60.309	176.200	H1 output mode cleaner line
131	575.9658	576.5057	61.943	53.805	——

threshold for signal detection, and outliers surpassing the threshold were considered present.

In an extended look, each outlier was sought in an expanded 20-day coherence time encompassing the original nine-day coherence time; the same assumption of signal continuity would predict, roughly, a doubling of the $2\mathcal{F}$ value for a doubling of coherence time. These cases as well were tested with software injections to determine a threshold.

In both time shifts and extended looks, the searches were conducted over a parameter space envelope obtained by starting at the outlier frequency parameters $(f, \dot{f}, \ddot{f}) \pm 2$ bins, and evolving those ranges backwards or forwards in time using the extremum values of the next derivative (e.g., f evolved at maximum $\dot{f}$, $\dot{f}$ evolved at maximum $\ddot{f}$) to achieve a conservatively wide envelope.

Outliers detected in time shifts and extended looks with joint $2\mathcal{F}$ greater than the threshold established by the software injections were labeled candidates. The time shift and extended look tests were not cumulative; an outlier needed only to survive any one test, not all of them, to persist as a candidate. The software injection threshold for both types of test was placed at a value for joint $2\mathcal{F}$ yielding 80% injection recovery; because each outlier would receive further consideration if it passed either test, the false dismissal probability for the first follow-up stage was ≈4%. The combined 323 outliers produced only seven candidates, listed in Table III.

These seven candidates were subject to manual follow up. They were compared to strain histograms of run-averaged (i.e., over all of S6) spectra from each detector, to identify instrumental noise lines which could be responsible. In five of the seven cases, the strain histograms gave clear evidence of an instrumental noise line responsible for the candidate, and in these cases records of prior detector characterization studies were consulted to provide

explanations for the noise artifacts. In those cases the artifact is listed in Table III as well. Two of the artifacts arose from hardware injections located at other points in the sky, used to test interferometer response [25].

The final remaining two candidates, which were not associated with known instrumental lines, were given another subsequent round of follow up: a time shift and extended look performed in data from June 2010, the farthest removed (in the time domain) available data of comparable sensitivity. The large time separation creates a large difference in the Doppler corrections needed to reconstruct an astrophysical source, making these corrections unlikely to reinforce instrumental or environmental artifacts. Both outliers failed to pass the $2\mathcal{F}$ thresholds established by software injections in any of their June tests.

The loudest $2\mathcal{F}$ value expected in the absence of signal depends on the number of templates searched [51][1]; for our search, the largest expected $2\mathcal{F}$ value lies in the range $72 \leq 2\mathcal{F} \leq 80$ with 90% confidence. The $2\mathcal{F}$ values associated with the two remaining candidates, outliers 79 and 131, were joint detector $2\mathcal{F} = 61.3$ and joint detector $2\mathcal{F} = 61.9$, respectively. The final two candidates' failure to pass the June tests and their marginal $2\mathcal{F}$ values led us to dismiss them as noise fluctuations.

For ease of understanding, Table IV illustrates the successive stages of follow up, and the number of remaining candidates after each step.

Thus no credible gravitational-wave signals were detected by our search. In the absence of a detection, we can set upper limits on the possible strength of gravitational waves in our data.

---

[1]The N_T templates used in our searches are not completely independent, but can be represented by N statistically independent templates where $N \approx 0.88 N_T$. See Sec. 8.7 of [51].

TABLE IV.   An illustration of the follow-up process, tracking the number of remaining candidates (and the nomenclature used for them in this paper) after each successive stage of follow up.

Follow-up stage	Remaining candidates (nomenclature)
Initial search	323 (outliers)
Time shifts + extended looks	7 (candidates)
Manual follow up: strain histograms	2 (candidates)
June data tests + loudest expected $2\mathcal{F}$	0 (candidates)

III. UPPER LIMITS

A. Methods

The method of setting upper limits was a variation on that used in [22] and [25]. This upper limit determination is based only of the $\mathcal{F}$-statistic and does not include additional criteria involved in candidate follow up. We split the frequency band into 0.1-Hz sub-bands, and for each of these used a semianalytic Monte Carlo method to estimate a 95% upper limit, defined as the strain h_0 at which our detection criterion would successfully detect 95% of signals. Due to the high computational cost of individually verifying all 5800 such sub-bands, these 0.1-Hz upper limit bands were consolidated into 1-Hz sub-bands. For each such 1-Hz band, we performed 1,000 software injections, split into eight groups of 125 signals. The strain h_0 of each group was $\pm5\%, \pm10\%, \pm15\%$, and $\pm20\%$ of the semi-analytic ULEs, respectively. A software injection was considered validated if it returned a value of $2\mathcal{F}$ greater than or equal to the loudest outlier in its 0.1-Hz sub-band, thus maintaining the original granularity. For each 1-Hz band, these 1,000 injections thus produced eight points on a detection efficiency curve. We then used a least-squares method to produce a sigmoid fit to the data
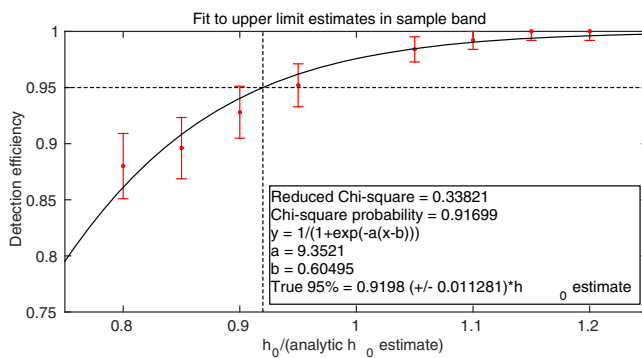

FIG. 1.   A demonstration of the upper limit validation technique for a sample band (101 Hz, October data). The x-axis is h_{nom}, h_0 divided by the ULE for this upper limit band; the eight points represent detection efficiencies for eight sets of 125 software injections. These eight points are then fit to a sigmoid curve (in black); the 95% upper limit can then be read off from the point where the curve crosses 95% detection efficiency.

TABLE V.   The twelve 0.1-Hz bands with outliers too large for the semianalytic method to converge to an estimate for h_0. These 0.1-Hz sub-bands were excluded from upper limit analysis; the quoted upper limits (Fig. 2) represent the remainder of their respective 1-Hz bands. The first column lists the affected 1-Hz band; the second column lists the respective vetoed 0.1-Hz sub-band; the third column lists the instrumental artifact identified using S6 run-averaged spectra.

Affected 1-Hz band	Vetoed 0.1-Hz sub-band	Artifact
180	180.0–180.1	Power mains harmonic
192	192.4–192.5	Hardware injection
217	217.5–217.6	Known instrumental artifact
234	234.0–234.1	Digital line (L1)
290	290.0–290.1	Digital line (L1)
370	370.1–370.2	L1 output mode cleaner line
393	393.1–393.2	Calibration line (H1)
396	396.7–396.8	Calibration line (L1)
400	400.2–400.3	H1 output mode cleaner line
403	403.8–403.9	L1 output mode cleaner line
417	417.1–417.2	H1 output mode cleaner line
580	580.0–580.1	Digital line (L1)

points, and from this curve determined a true 95% upper limit, defined as the value of h_0 at which the fitting curve intersected 95% efficiency. Figure 1 shows such a plot for a sample band. In cases where the 95% point was extrapolated (as opposed to interpolated) from the eight points, and in cases where the uncertainty on the 95% point was greater than 5%, a new set of eight points was generated using the 95% point as the initial h_0 estimate and a 95% point was determined from the combined sets (e.g., a curve was fit to 16 points after one rerun, 24 points after two reruns, etc.).

A small number of 0.1-Hz bands had outliers so large that the semianalytic method failed to converge to an estimate for h_0. Instrumental artifacts at these frequencies were identified using S6 run-averaged spectra and the respective 1-Hz bands were then rerun with the disturbed 0.1-Hz sub-band excluded. The excluded bands are detailed in Table V.

B. Results

Figure 2 shows the 95% confidence ULs over the full band for the July–August data set, which was the more sensitive of the two because of its much greater livetime (642 SFTs vs 374 SFTs for the October data set). The blue curve represents the expected sensitivity of the search for this data set, computed from the power spectral density at each frequency; there is good agreement with the ULs. The black line represents the age-based limit derived when first considering the parameter space. Its intersection with the ULs at either end of the plot is a confirmation that we correctly estimated the frequency band to search over.
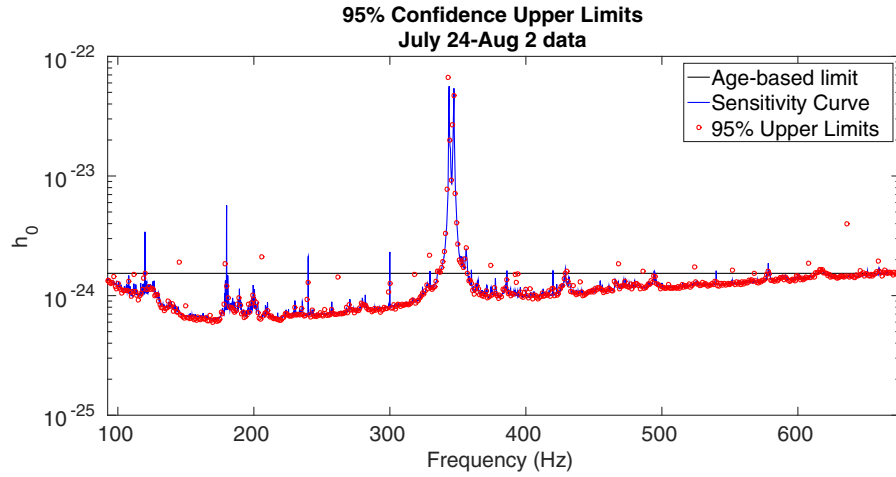
FIG. 2. Upper limits at 95% confidence (red circles) compared to the upper limit estimate curve of the detector (blue curve) and the initial age-based limit on h_0 (black line). The upper limit estimate curve is based on Eq. (5) over the 9.2 days of coherence time, corrected for detector livetime and sky location and summed over detectors in inverse quadrature.

Figure 3 is a similar plot converting the upper limits on h_0 to upper limits on fiducial ellipticity ϵ, using the formula [52]

$$\epsilon = \frac{c^4}{4\pi^2 G} \frac{d}{I_{zz} f^2} h_0. \qquad (12)$$

The black curve represents the age-based limit on fiducial ellipticity, using the same assumptions (braking index $n = 5$, age $\tau = 300$ years) used in the parameter space calculations.

The amplitude α of r-mode oscillations in a neutron star is related to the gravitational-wave strain amplitude h_0 by [53]

$$\alpha = 0.028 \left(\frac{h_0}{10^{-24}}\right) \left(\frac{r}{1 \text{ kpc}}\right) \left(\frac{100 \text{ Hz}}{f}\right)^3. \qquad (13)$$
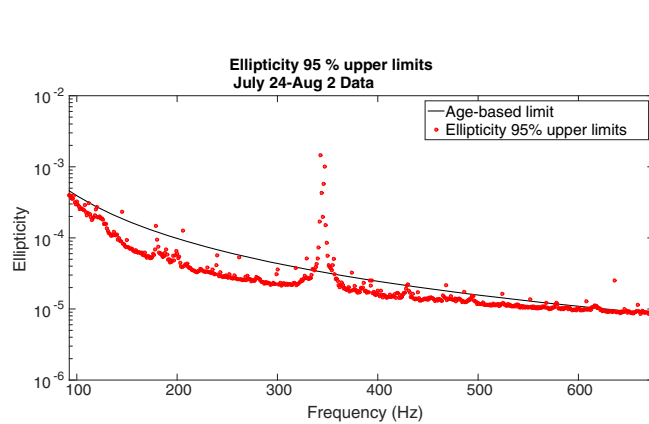
Figure 4 uses this formula to convert the upper limits on h_0 to upper limits on the r-mode amplitude α. The black curve represents the age-based limit on α, under the same age assumptions used for h_0 and ellipticity, but with $n = 7$, which characterizes r-mode emission. In all three plots, the age-based limit is beaten everywhere the upper limits lie below the black curve.

IV. DISCUSSION

This search has placed the first explicit upper limits on continuous gravitational-wave strength from the nearby globular cluster NGC 6544 for spin-down ages as young as 300 years, and is the first directed CW search for any globular cluster. The most stringent upper limits on strain (h_0^{UL}) obtained were $h_0^{\text{UL}} = 6.7 \times 10^{-25}$ for the 173–174 Hz band in the October data set, and $h_0^{\text{UL}} = 6.0 \times 10^{-25}$ for the 170–171 Hz band in the July–August data.
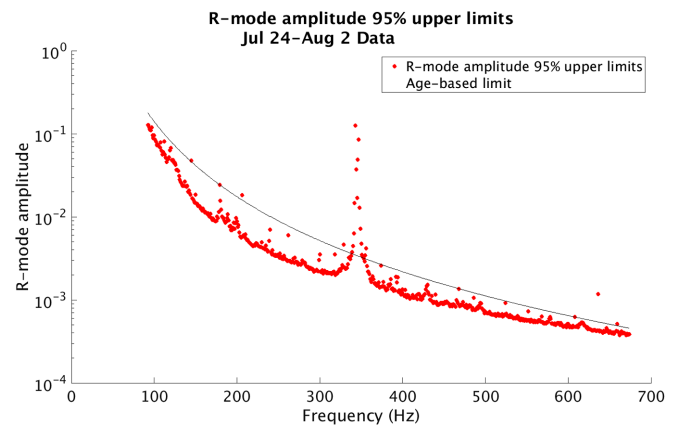

FIG. 3. Upper limits at 95% confidence (red circles) compared to the initial age-based limit on fiducial ellipticity ϵ (black line).

FIG. 4. Upper limits at 95% confidence (red circles) compared to the initial age-based limit on r-mode amplitude α (black line).

The best upper limit is comparable to the best upper limit of 7×10^{-25} at 150 Hz obtained by the Cas A search [22]; the recent search over nine supernova remnants, done without resampling [25], set upper limits as low as 3.7×10^{-25} for the supernova remnant $G93.3 + 6.9$, but used a coherence time of over 23 days (and a frequency band of only 264 Hz). The same analysis set a comparable 95% upper limit of 6.4×10^{-25} for the supernova remnant $G1.9 + 0.3$, as expected given its similar declination and the search's similar coherence time (9.2 days for NGC 6544 vs 9.1 days for $G1.9 + 0.3$). Note, however, that the $G1.9 + 0.3$ search was limited to a 146 Hz search band, compared to 583 Hz for NGC 6544. The search reported here was carried out at substantially less computational cost because of barycentric resampling, and could thus search over a much larger parameter space.

The best upper limit on fiducial ellipticity, established using the July–August data set, was $\epsilon = 8.5 \times 10^{-6}$, for the 1-Hz band starting at 670 Hz. This is comparable to the best upper limit (4×10^{-5}) obtained by the Cas A search [51]; the supernova remnant search [25] set a comparable upper limit on fiducial ellipticity at 7.6×10^{-5} for the supernova remnant $G1.9 + 0.3$.

These ellipticities are within the range of maximum theoretical ellipticities predicted for stars with some exotic phases in the core [54,55], and the lowest of them is achievable for purely nucleonic stars with a sufficiently stiff equation of state and low mass [55]. Hence the search could have detected some exotic stars if they were supporting close to their maximum possible ellipticity; however, the lack of a detection cannot be used to infer constraints on the composition of any star, since the deformation could be much less than its maximum supportable value.

The first observing run of the Advanced LIGO detectors began in September 2015 [56] and the sensitivity of the detectors is already three times or more better than that used in this search, with an order of magnitude improvement over S6 expected eventually [57]. The barycentric resampling algorithm first implemented in this search is being used extensively in CW searches in the advanced detector era; it has been integrated into the search codes for both coherent searches (like the supernova remnant search) [58] and semicoherent searches (Einstein@Home).

ACKNOWLEDGMENTS

[1] B. Abbott *et al.*, Phys. Rev. D **69**, 082004 (2004).
[2] B. Abbott *et al.*, Phys. Rev. Lett. **94**, 181103 (2005).
[3] B. Abbott *et al.*, Phys. Rev. D **76**, 042001 (2007).
[4] B. Abbott *et al.*, Astrophys. J. **683**, L45 (2008).
[5] J. Abadie *et al.*, Astrophys. J. **737**, 93 (2011).
[6] B. P. Abbott *et al.*, Astrophys. J. **713**, 671 (2010).
[7] J. Aasi *et al.*, Astrophys. J. **785**, 119 (2014).
[8] B. Abbott *et al.*, Phys. Rev. D **72**, 102004 (2005).
[9] B. Abbott *et al.*, Phys. Rev. D **76**, 082001 (2007).
[10] B. Abbott *et al.*, Phys. Rev. D **77**, 022001 (2008).

[11] B. Abbott *et al.*, Phys. Rev. D **79**, 022001 (2009).
[12] B. P. Abbott *et al.*, Phys. Rev. Lett. **102**, 111102 (2009).
[13] B. P. Abbott *et al.*, Phys. Rev. D **80**, 042003 (2009).
[14] J. Abadie *et al.*, Phys. Rev. D **85**, 022001 (2012).
[15] J. Aasi *et al.*, Phys. Rev. D **87**, 042001 (2013).
[16] J. Aasi *et al.*, Classical Quantum Gravity **31**, 085014 (2014).
[17] J. Aasi *et al.*, Classical Quantum Gravity **31**, 165014 (2014).
[18] J. Aasi *et al.*, Phys. Rev. D **90**, 062010 (2014).
[19] B. Knispel and B. Allen, Phys. Rev. D **78**, 044031 (2008).
[20] B. Abbott *et al.*, Phys. Rev. D **76**, 082003 (2007).
[21] J. Abadie *et al.*, Phys. Rev. Lett. **107**, 271102 (2011).
[22] J. Abadie *et al.*, Astrophys. J. **722**, 1504 (2010).
[23] K. Wette *et al.*, Classical Quantum Gravity **25**, 235011 (2008).
[24] J. Aasi *et al.*, Phys. Rev. D **88**, 102002 (2013).
[25] J. Aasi *et al.*, Astrophys. J. **813**, 39 (2015).
[26] A. G. Lyne and F. Graham-Smith, *Pulsar Astronomy*, 3rd ed. (Cambridge University Press, Cambridge, 2006).
[27] P. Jaranowski, A. Krolak, and B. F. Schutz, Phys. Rev. D **58**, 063001 (1998).
[28] C. Cutler and B. F. Schutz, Phys. Rev. D **72**, 063006 (2005).
[29] R. Prix and B. Krishnan, Classical Quantum Gravity **26**, 204013 (2009).
[30] LAL/LALapps Software Suite, http://www.lsc-group.phys .uwm.edu/daswg/projects/lalsuite.html, Tag: CFSv2_ singleIFO_DKOrder_for_real.
[31] P. Astone, K. M. Borkowski, P. Jaranowski, M. Pietka, and A. Królak, Phys. Rev. D **82**, 022005 (2010).
[32] P. Patel, X. Siemens, R. Dupuis, and J. Betzwieser, Phys. Rev. D **81**, 084032 (2010).
[33] P. Patel, Ph.D. thesis, California Institute of Technology, 2010.
[34] Z.-X. Wang, D. Chakrabarty, and D. L. Kaplan, Nature (London) **440**, 772 (2006).
[35] A. Wolszczan and D. A. Frail, Nature (London) **355**, 145 (1992).
[36] S. E. Thorsett, Z. Arzoumanian, and J. H. Taylor, Astrophys. J. Lett. **412**, L33 (1993).
[37] S. Sigurdsson, H. B. Richer, B. M. Hansen, I. H. Stairs, and S. E. Thorsett, Science **301**, 193 (2003).
[38] S. Sigurdsson, Astrophys. J. Lett. **399**, L95 (1992).
[39] M. Vigelius and A. Melatos, Mon. Not. R. Astron. Soc. **395**, 1985 (2009).
[40] B. Haskell, M. Priymak, A. Patruno, M. Oppenoorth, A. Melatos, and P. D. Lasky, Mon. Not. R. Astron. Soc. **450**, 2393 (2015).
[41] F. Verbunt and P. Hut, in *The Origin and Evolution of Neutron Stars*, edited by D. J. Helfand and J.-H. Huang (IAU Symposium, 1987), Vol. 125, p. 187.
[42] W. E. Harris, Astron. J. **112**, 1487 (1996).
[43] W. E. Harris, arXiv:1012.3224.
[44] K. Wette, Phys. Rev. D **85**, 042003 (2012).
[45] D. M. Whitbeck, Ph.D. thesis, The Pennsylvania State University, 2006.
[46] R. Prix, Phys. Rev. D **75**, 023004 (2007).
[47] B. J. Owen, Phys. Rev. D **53**, 6749 (1996).
[48] P. R. Brady, T. Creighton, C. Cutler, and B. F. Schutz, Phys. Rev. D **57**, 2101 (1998).
[49] D. Heggie and P. Hut, *The Gravitational Million-Body Problem: A Multidisciplinary Approach to Star Cluster Dynamics* (Cambridge University Press, Cambridge, 2003).
[50] D. Keitel, R. Prix, M. A. Papa, P. Leaci, and M. Siddiqi, Phys. Rev. D **89**, 064023 (2014).
[51] K. Wette, Ph.D. thesis, Australian National University, 2009.
[52] P. Saulson, *Fundamentals of Interferometric Gravitational-Wave Detectors* (World Scientific Publishing Company, Incorporated, Singapore, 1994).
[53] B. J. Owen, Phys. Rev. D **82**, 104002 (2010).
[54] B. J. Owen, Phys. Rev. Lett. **95**, 211101 (2005).
[55] N. K. Johnson-McDaniel and B. J. Owen, Phys. Rev. D **88**, 044004 (2013).
[56] B. P. Abbott *et al.*, Living Rev. Relativ. **19** (2016).
[57] LIGO Scientific Collaboration *et al.*, Classical Quantum Gravity **32**, 074001 (2015).
[58] A. Idrisy, Ph.D. thesis, The Pennsylvania State University, 2015.